THE JOURNAL OF PHYSICAL CHEMISTRY Letters

Letter

Cite This: J. Phys. Chem. Lett. 2019, 10, 1037−1042

pubs.acs.org/JPCL

Room-Temperature Phosphorescence from Metal-Free Organic Materials in Solution: Origin and Molecular Design

Anqi Lv,[†,∥] Wenpeng Ye,[†,∥] Xueyan Jiang,[†] Nan Gan,[†] Huifang Shi,[†] Wei Yao,[†] Huili Ma,*[,†] Zhongfu An,*[,†] and Wei Huang*[,†,‡]

[†]Key Laboratory of Flexible Electronics (KLOFE) & Institute of Advanced Materials (IAM), Nanjing Tech University (NanjingTech), 30 South Puzhu Road, Nanjing 211816, People's Republic of China

[‡]Institute of Flexible Electronics (IFE), Northwestern Polytechnical University (NPU), 127 West Youyi Road, Xi'an 710072, People's Republic of China

Supporting Information

ABSTRACT: Metal-free organic materials with room-temperature phosphorescence (RTP) is hardly achieved in solution owing to the ambiguous underlying mechanism. By combining thermal vibration correlation function rate theory and a polarizable continuum model (PCM) coupled with the Tamm−Dancoff approximation method, concentrating on β-hydroxyvinylimine boron compounds C-BF_2 and S-BF_2, we showed that the increased intersystem crossing (k_{isc}) and radiative decay rates (k_p) are responsible for the strong RTP of S-BF_2 in solution. From C-BF_2 to S-BF_2, the T_2 state is increasingly dominated by the n → π* transition, largely enhancing the k_{isc} of $S_1 \rightarrow T_2$ (up to 3 orders of magnitude) and k_p of $T_1 \rightarrow S_0$. Impressively, the nonradiative decay rate of $T_1 \rightarrow S_0$ is slightly increased by suppressing the out-of-plane twisting motions. This mechanism is also tenable for several designed RTP molecules through further experimental demonstration, which will pave a new way to design organic materials with single-molecule phosphorescence for applying to organic light-emitting diodes.

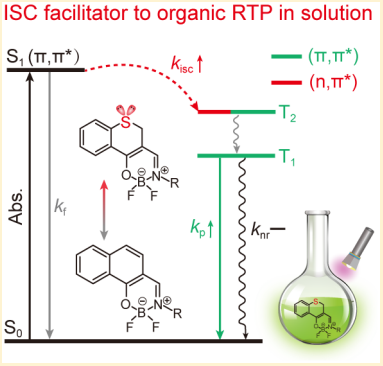

Organic room-temperature phosphorescence (RTP) materials have evoked considerable attention owing to natural advantages in aspects of chemical sensors, bioimaging, and so on.[1−9] Unlike the traditional organometallic complexes, which emitted bright RTP in solution that benefited from the heavy-atom accelerated intersystem crossing (ISC) process between singlet and triplet excited states,[10,11] the metal-free organic molecules were generally known as nonphosphorescence at room temperature due to the slow ISC process and fast depopulation of triplet excitons caused by active molecular motions. To date, the metal-free organic materials with RTP were usually achieved in the crystalline phase.[12−20] However, the use of crystals significantly limits the practical applications and functionalization of the compounds, owing to the difficult processing and unmanageable molecular packing in crystal forms. To avoid this issue, many efforts have been devoted to achieve RTP in solution for organic materials through the introduction of halogen atoms and heteroatoms.[21−27] The β-hydroxyvinylimine boron derivatives, as an extensible system, showed bright RTP in solution,[23,24] which has been attributed to the improved population of triplet exactions by a singlet fission process[23] or the enhanced ISC process of $S_1{}^1(n, \pi^*) \rightarrow T_1{}^3(\pi, \pi^*)$ owing to sulfur substitution.[24] Namely, it is still a formidable challenge to clarify the underlying mechanism in metal-free organic RTP materials in solution. However, the excited-state transition has proved to be a crucial factor to understand the solid RTP in organic materials,[28,29] and this provides a clue to reveal the underlying mechanism in RTP from organic materials in solution.

Herein, we focus on the change in excited states of two β-hydroxyvinylimine boron molecules, named as C-BF_2 and S-BF_2 (see Figure 1). Through a combination of thermal

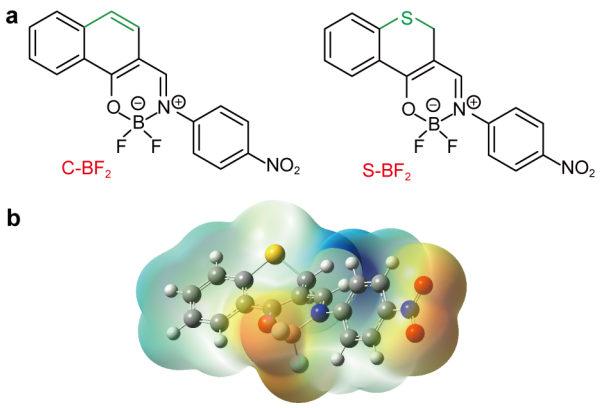

Figure 1. Chemical structure of (a) β-hydroxyvinylimine boron compounds (C-BF_2 and S-BF_2) and (b) setup of the PCM (taking S-BF_2 as an example).

Received: January 24, 2019
Accepted: February 18, 2019
Published: February 18, 2019

DOI: 10.1021/acs.jpclett.9b00221
J. Phys. Chem. Lett. 2019, 10, 1037−1042

vibrational correlation function rate theory and a linear-response polarizable continuum model (PCM) within the Tamm−Dancoff approximation (TDA) method, we found that from C-BF_2 to S-BF_2 the sulfur atom introduces an increasing n → π^* transition into the T_2 state, resulting in a hugely accelerated ISC rate of $S_1 \rightarrow T_2$ and an enhanced radiative decay rate (k_p) of $T_1 \rightarrow S_0$. However, it has little influence on the nonradiative decay rate of $T_1 \rightarrow S_0$ due to the almost unchanged T_1 state. Consequently, the efficient RTP in S-BF_2 was observed in solution. Impressively, this mechanism has been successfully implemented in designing organic RTP molecules in solution, which was further confirmed by experimental data, and paves a new way to design efficient organic RTP materials in solution.

Electronic Structure of the Low-Lying Excited States. Phosphorescence is the transition between excited states with different spin multiplicity. Subsequently, the singlet and triplet excited states of the β-hydroxyvinylimine boron compounds (C-BF_2 and S-BF_2) were evaluated by the TDDFT method, and the solvent effect of CH_2Cl_2 was modeled by using the PCM. Moreover, TDA calculations were also performed to ensure the stability of the triplet state.[30−32] Because of the dependence of these BODIPY derivatives on the XC functional,[33,34] a series of XC functionals, including B3LYP, PBE0, BMK, M06-2X, CAM-B3LYP, and ωB97X-D, were used to evaluate the excitation energies of the T_1 state (Table S1) together with the 6-31G(d) basis set. We then found that the calculated T_1 excitation energy of S-BF_2 (2.21 eV) at the TDA/BMK/6-31G(d) level is very consistent with the experimental value (2.16 eV), with a tiny deviation of 0.05 eV. Therefore, it is a preferred method to calculate the excited-state properties of the current organic RTP molecules.

To clarify the mechanism underlying the RTP of the metal-free β-hydroxyvinylimine boron compounds in solution, their excited-state electronic structures were then calculated at the level of TDA/BMK/6-31G(d), including the excitation energies, nature transition orbitals (NTOs) and spin−orbit coupling (SOC) constants (ξ), as shown in Figure 2. When focusing on the change in excited states from fluorescent molecule C-BF_2 to phosphorescent molecule S-BF_2, we found the following points: (i) the SOC values between S_1 and T_n (n = 1,2) are significantly enlarged with about 1 order of magnitude. For example, the value of $\xi(S_1, T_2)$ is hugely increased from 1.70 cm^{-1} in C-BF_2 to 14.17 cm^{-1} in S-BF_2, and it can be understood by the uptrend of γ from 0.0% in C-BF_2 to 2.13% in S-BF_2 based on our previous work.[27] Such a change is obviously attributed to the occurrence of the n → π^* transition in S_1 (with a proportion of 1.87%) and T_2 states (with a proportion of 6.45%) of S-BF_2,[26] thereby resulting in a large SOC constant according to El-Sayed's rule.[35] In a word, the increase of SOC not only promotes the ISC process of $S_1 \rightarrow T_n$ but also facilitates the enhancement of the radiative decay channel of $T_1 \rightarrow S_0$. These features are then responsible for the generation of efficient RTP in solution. (ii) The value of $\xi(T_1, S_0)$ is increased only 3-fold from 2.97 cm^{-1} in C-BF_2 to 8.99 cm^{-1} in S-BF_2; this may be ascribed to the increase of atomic weight from carbon to sulfur atoms[14] because the T_1 state remains almost unchanged (β is equal to 100% for all molecules; see Table S2). However, the increased SOC implies a promoting ISC channel of $T_1 \rightarrow S_0$, which is harmful to the production of RTP. Beyond the electronic transition, the electron−vibration coupling may give a clue to this exception.

Decay Rates between Singlet and Triplet Excited States. It is known that the radiative decay (k_p) and ISC rates (k_{isc}) between singlet and triplet excited states are essential for phosphorescence. The former can be simply estimated through Einstein spontaneous emission, while the latter k_{isc} is calculated by using the MOMAP program.[34] When going from C-BF_2 to S-BF_2, Table 1 and Figure S1 show that the k_{isc} of $S_1 \rightarrow T_2$ is largely enhanced by 3 orders of magnitude, from 8.71×10^6 to 5.94×10^9 s^{-1}, mainly owing to the increased n → π^* transition in the T_2 state. However, the nonradiative decay rate k_{nr} has a slight enlargement from 1.77×10^4 to 4.13×10^4 s^{-1}, and the radiative decay rate k_p is clearly increased from 0.96 to 22.77 s^{-1} due to the enhanced SOC values of $S_1 \rightarrow T_n$ (see Figure 2). Impressively, the calculated phosphorescence lifetime of 24.21 μs is in good accordance with the experimental value (8.30 μs). These results indicate that the greatly increased ISC rate k_{isc} and radiative decay rates k_p are responsible for the strong RTP of S-BF_2 in solution, when a sulfur atom is incorporated.

Table 1. Calculated ISC Rate k_{isc} of $S_1 \rightarrow T_2$ and Radiative k_p and Nonradiative Decay Rates k_{nr} of $T_1 \rightarrow S_0$ for C-BF_2 and S-BF_2[a]

	$S_1 \rightarrow T_2$	$T_1 \rightarrow S_0$		τ (μs)	
	k_{isc} (s^{-1})	k_p (s^{-1})	k_{nr} (s^{-1})	calcd	exptl
C-BF_2	8.71×10^6	0.96	1.77×10^4		
S-BF_2	5.94×10^9	22.77	4.13×10^4	24.21	8.30

[a]The experimental data are also shown as a comparison.[24]

In order to get a closer look at such a large change, the ISC rate is simplified as $k_{isc} \propto |\xi|^2 \exp(-E/\lambda)$ under short-time and high-temperature approximations,[37,38] namely, the ISC rate primarily determined by the SOC constant (ξ) and electron−vibration coupling that can be characterized by the normal-mode reorganization energy, λ, as well as the energy gap E between two states. Consequently, the increase of 3 orders of magnitude in k_{isc} of $S_1 \rightarrow T_2$ from C-BF_2 to S-BF_2 can be divided into two parts. One part is the contribution of SOC with 2 orders of magnitude (see Figure 2), and the other part is the contribution of the reorganization energy with 1 order of magnitude. This was further confirmed by the largely enhanced

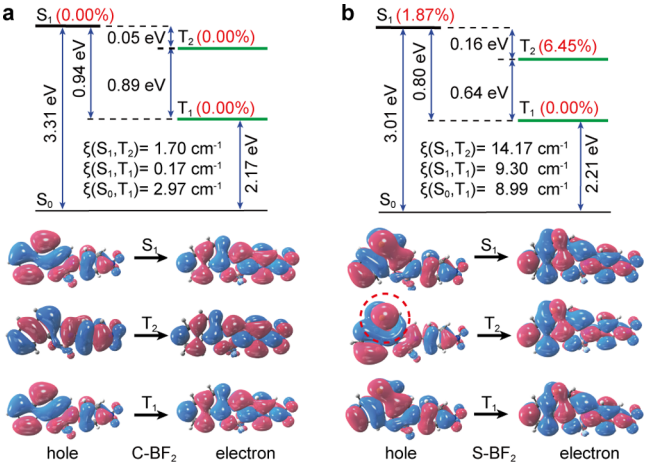

Figure 2. Calculated energy diagram, spin−orbit coupling (SOC) constants (ξ), and nature transition orbitals (NTOs) for (a) C-BF_2 and (b) S-BF_2 in CH_2Cl_2 solution at the level of TDA/BMK/6-31G(d).

DOI: 10.1021/acs.jpclett.9b00221
J. Phys. Chem. Lett. 2019, 10, 1037−1042

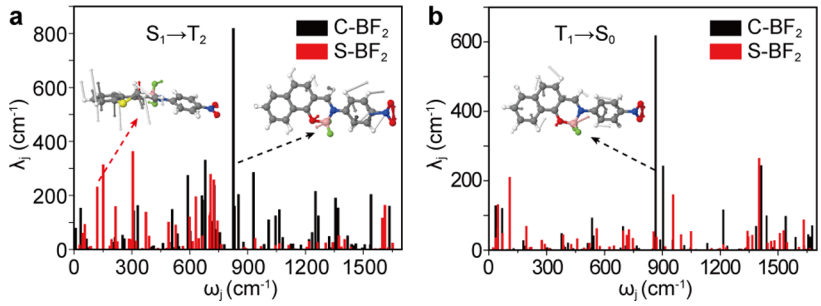

Figure 3. Calculated λ_j versus ω_j in transitions of (a) $S_1 \rightarrow T_2$ and (b) $T_1 \rightarrow S_0$ for C-BF_2 and S-BF_2.

reorganization energies in the low-frequency region (<200 cm^{-1}) from C-BF_2 to S-BF_2, which govern the k_{isc} derived from λ, and they are mainly assigned to out-of-plane twisting motions (see Figure 3a). However, for the k_{nr} of $T_1 \rightarrow S_0$, it has only a 2-fold increase from C-BF_2 to S-BF_2, as seen from Table 1. This is in conflict with the expectation that the k_{nr} at least should be increased by about 1 order of magnitude owing to the 3-fold increase in $\xi(T_1, S_0)$ from 2.97 cm^{-1} in C-BF_2 to 8.99 cm^{-1} in S-BF_2 (see Figure 2). This deviation can be well explained by the reduced reorganization energy from 2821.01 cm^{-1} in C-BF_2 to 2396.02 cm^{-1} in S-BF_2, such as the large breathing vibration in C-BF_2 (see Figure 3b). Namely, the negative change in λ may offset the positive contribution of SOC to k_{nr}.

When further projecting the reorganization energies into the internal coordinate relaxation of the molecules (see Figure 4),

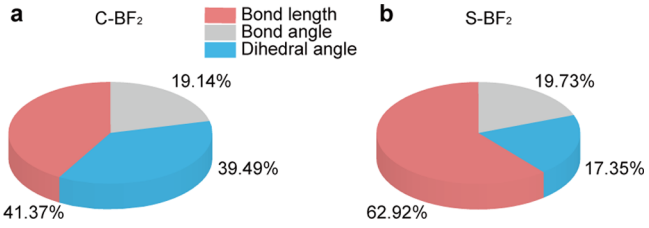

Figure 4. Contributions to the total reorganization energy from the bond length, bond angle, and dihedral angle for (a) C-BF_2 and (b) S-BF_2.

it is found that from C-BF_2 to S-BF_2 the contributions from the dihedral angle relating to the out-of-plane twisting motions are reduced from 39.49 to 17.35%, while the contributions originating from bond length associated with the intramolecular stretching vibration are increased from 41.37% in C-BF_2 to 62.92% in S-BF_2, and the contributions derived from the bond angle are barely changed with a value of ca. 19%. We then deduced that the introduction of a sulfur atom can restrain the out-of-plane molecular motion, which reduces the enlargement of k_{nr} induced by the weak SOC.

Extendable Organic RTP Molecules in Solution with ISC Facilitator. Up to now, metal-free organic materials with RTP in solution are still a very special case in view of the fast ISC channel in S-BF_2 when introducing a sulfur atom, which can be used as an ISC facilitator to alleviate this predicament. Four molecules (**1**−**4**) can then be designed by substitution of the nitrobenzene unit in S-BF_2, as shown in Figure 5a. Theoretical calculations indicated that the large SOC values between S_1 and T_2 in these molecules (Figures 5 and S2) will make a fast ISC channel and result in bright RTP in solution. For example, the value of $\xi(S_1, T_2)$ in molecule **2** is large at 16.29 cm^{-1} in S-BF_2, which was attributed to the increased n → π^* transition (11.54%) in the T_2 state (Figure 5b). Similar results have also been obtained in other molecules; see Figures S2 and S3. Experiments further confirmed this point. As seen from Figure 5c,d, the measured photoluminescence (PL) spectrum of molecule **2** showed a maximum wavelength at 545 nm with a lifetime of 9.22 μs in dilute CH_2Cl_2 solution, which was thus assigned to phosphorescence emission. Therefore, we proposed that the S-BF_2 group can act as an ISC facilitator to design metal-free organic RTP materials in solution.

In summary, we have revealed the underlying mechanism in metal-free organic RTP materials in solution and proposed an extendable molecular design strategy. By using thermal vibration correlation function rate theory coupled with TDA calculations, we have investigated the excited-state nature of β-hydroxyvinylimine boron compounds in solution, including excitation energies, SOC constants, and decay rates between singlet and triplet states. It is concluded that the contributions of the n → π^* transition to the T_2 state become difficult to ignore when a heteroatom is introduced into β-hydroxyvinylimine boron compounds. Such a change not only results in a hugely increased ISC rate of $S_1 \rightarrow T_2$, up to 3 orders of magnitude for S-BF_2, but also facilitates the radiative decay rate k_p of $T_1 \rightarrow S_0$. However, the nonradiative decay rate k_{nr} of $T_1 \rightarrow S_0$ has a slight increase due to suppression of the out-of-plane twisting motion by the sulfur atom, which reduces the positive contributions of SOC to k_{nr}. Consequently, a strong RTP was observed in metal-free β-hydroxyvinylimine boron compounds in solution with the introduction of heteroatoms. Furthermore, several molecules with efficient RTP in solution were successfully designed and confirmed by theoretical and experimental works. Therefore, the present mechanism provides a good understanding and strategy for the design and development of metal-free organic RTP materials in solution.

METHODOLOGICAL APPROACH

Computational Details. Geometry optimization and harmonic vibrational frequency calculations of the ground (S_0) and the low-lying triplet excited states (T_1 and T_2) were performed at the (TD)B3LYP/6-31G(d) level. The bulk solvent effect was modeled by using the integral equation formalism (IEF) of the linear-response polarizable continuum model (PCM)[39,40] implemented in the C.01 version of the Gaussian 09 package.[41] The C-BF_2, S-BF_2, and molecules **1**−**4** were modeled in dichloromethane (CH_2Cl_2) solution as BODIPY derivatives, whose excitation energies have a high sensitivity to the exchange−correlation (XC) functional.[33,34] Hence, a wide panel of XC functionals, including B3LYP, PBE0, BMK, M06-2X, CAM-B3LYP, and ωB97X-D, were used to evaluate the

DOI: 10.1021/acs.jpclett.9b00221
J. Phys. Chem. Lett. 2019, 10, 1037−1042

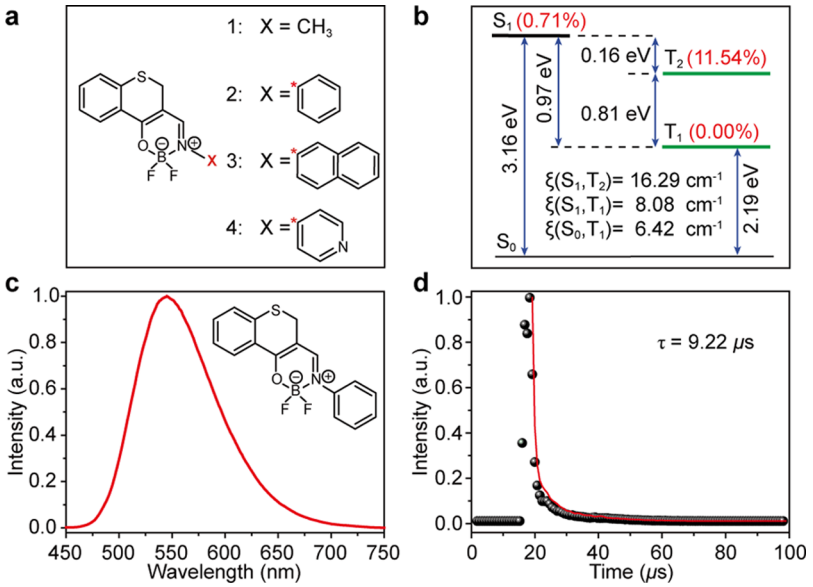

Figure 5. (a) Molecular structures of boron compounds **1**−**4**. (b) Calculated energy diagram and SOC constants (ξ) for molecule **2** in CH_2Cl_2 solution at the TDA/BMK/6-31G(d) level. (c) Steady-state photoluminescence (PL) spectra of molecule **2** in 1×10^{-5} M CH_2Cl_2 solution. (d) PL decay curves of molecule **2** at 545 nm in CH_2Cl_2 solution in air at 298 K.

excitation energy of the T_1 state based on time-dependent density functional theory (TDDFT). while the Tamm−Dancoff approximation (TDA) within TDDFT was also performed in consideration of the instability of triplet states.[30−32] It was found that the calculated excitation energies by TDA/BMK/6-31G(d) agree well with the experimental value, which was then used to find the nature transition orbitals (NTO) of singlet and triplet states and the spin−orbit coupling (SOC) constants by coupling with the Pysoc code.[42] The Mulliken population analysis (MPA) was implemented to calculate the proportions of n → π^* (α) and $\pi \rightarrow \pi^*$ (β) transition in excited states using the Multiwfn package;[43] subsequently, $\gamma = S_1(\alpha) \times T_2(\beta)$ was also evaluated based on our previous work.[29]

The phosphorescence is determined by two processes: (i) the ISC rate (k_{isc}) of $S_1 \rightarrow T_n$ and (ii) the radiative decay (k_p) and nonradiative decay rates (k_{nr}) of $T_1 \rightarrow S_0$; k_{nr} is generally dominated by k_{isc} of $T_1 \rightarrow S_0$ when other decay channels are ignored. The ISC rates (k_{isc}) between singlet and triplet excited states were evaluated by thermal vibration correlation function rate theory using the MOMAP program.[36] It is noted that the Cartesian coordinate was used to calculate the reorganization energies $\lambda_j = \Delta Q_j \omega_j^2/2\hbar$ (where ω_j is the normal-mode frequency and ΔQ_j is the normal mode displacement between initial and final states); the Duschinsky rotation effect was neglected. The k_p of $T_1 \rightarrow S_0$ was estimated by Einstein's spontaneous emission rate $k_p = \frac{E^2 f}{1.499\ \mathrm{cm^{-2}\cdot s}}$, where E is the vertical excitation energy and $f = \frac{2}{3}E|\mu|^2$ is the oscillator strength. The transition dipole moment μ of $T_1 \rightarrow S_0$ can be expressed as[44]

$$\mu_{T1\rightarrow S0} = \sum_k \frac{\langle S_0|\hat{\mu}|S_k\rangle\langle S_k|\hat{H}_{SOC}|T_1\rangle}{{}^3E_{T1} - {}^1E_{Sk}} + \sum_n \frac{\langle S_0|\hat{H}_{SOC}|T_n\rangle\langle T_n|\hat{\mu}|T_1\rangle}{{}^1E_{S0} - {}^3E_{Tn}} \quad (1)$$

where n and k (here $n = 10$, $k = 5$) are the intermediate triplet and singlet electronic states.

Synthesis and Characterizations. 2,2-Difluoro-3-phenyl-2*H*,5*H*-2λ^4,3λ^4-thiochromeno[3,4-*e*][1,3,2]oxazaborinine (S-BF_2-B, the so-called molecule **2**) was synthesized through three-step reactions, as shown in Scheme S1.[24] The chemical structure of target molecule **2** was fully characterized by a ^{13}C NMR spectrum and a ^1H NMR spectrum (see Figures S4 and S5).

■ ASSOCIATED CONTENT

Supporting Information

The Supporting Information is available free of charge on the ACS Publications website at DOI: 10.1021/acs.jpclett.9b00221.

Calculated nature of the excited state, including the excitation energy, nature transition orbitals, spin−orbit coupling, and decay rates, for C-BF_2, S-BF_2, and molecules **1**−**4**, and chemical structure and synthesis processes for molecule **2** (PDF)

■ AUTHOR INFORMATION

Corresponding Authors

*E-mail: iamhlma@njtech.edu.cn (H.M.).
*E-mail: iamzfan@njtech.edu.cn (Z.A.).
*E-mail: iamwhuang@njtech.edu.cn (W.H.).

ORCID

Huili Ma: 0000-0003-0332-2999
Zhongfu An: 0000-0002-6522-2654

Author Contributions

‖A. Lv and W. Ye contributed equally.

Notes

The authors declare no competing financial interest.

■ ACKNOWLEDGMENTS

This work is supported by the National Natural Science Foundation of China (91833302, 91833304, 21875104,

DOI: 10.1021/acs.jpclett.9b00221
J. Phys. Chem. Lett. 2019, 10, 1037−1042

51673095, and 61605074), the National Basic Research Program of China (973 Program, No. 2015CB932200), the Natural Science Fund for Distinguished Young Scholars of Jiangsu Province (BK20180037), the Natural Science Fund for Colleges and Universities (17KJB430020), and "High-Level Talents in Six Industries" (XCL-025) of Jiangsu Province and a Nanjing Tech Start-up Grant (3983500201, 3983500158, and 3983500169). We are grateful to the High Performance Computing Center in Nanjing Tech University for supporting the computational resources.

REFERENCES

(1) Fermi, A.; Bergamini, G.; Roy, M.; Gingras, M.; Ceroni, P. Turn-on Phosphorescence by Metal Coordination to a Multivalent Terpyridine Ligand: A New Paradigm for Luminescent Sensors. *J. Am. Chem. Soc.* **2014**, *136*, 6395−6400.

(2) Kwon, M. S.; Jordahl, J. H.; Phillips, A. W.; Chung, K.; Lee, S.; Gierschner, J.; Lahann, J.; Kim, J. Multi-Luminescent Switching of Metal-Free Organic Phosphors for Luminometric Detection of Organic Solvents. *Chemi. Sci.* **2016**, *7*, 2359−2363.

(3) Zhen, X.; Tao, Y.; An, Z.; Chen, P.; Xu, C.; Chen, R.; Huang, W.; Pu, K. Ultralong Phosphorescence of Water-Soluble Organic Nanoparticles for In Vivo Afterglow Imaging. *Adv. Mater.* **2017**, *29*, 1606665.

(4) Nicol, A.; Kwok, R. T. K.; Chen, C.; Zhao, W.; Chen, M.; Qu, J.; Tang, B. Z. Ultrafast Delivery of Aggregation-Induced Emission Nanoparticles and Pure Organic Phosphorescent Nanocrystals by Saponin Encapsulation. *J. Am. Chem. Soc.* **2017**, *139*, 14792−14799.

(5) Fateminia, S. M. A.; Mao, Z.; Xu, S.; Yang, Z.; Chi, Z.; Liu, B. Organic Nanocrystals with Bright Red Persistent Room-Temperature Phosphorescence for Biological Applications. *Angew. Chem., Int. Ed.* **2017**, *56*, 12160−12164.

(6) Miao, Q.; Xie, C.; Zhen, X.; Lyu, Y.; Duan, H.; Liu, X.; Jokerst, J. V.; Pu, K. Molecular Afterglow Imaging with Bright, Biodegradable Polymer Nanoparticles. *Nat. Biotechnol.* **2017**, *35*, 1102−1110.

(7) Cheng, Z.; Shi, H.; Ma, H.; Bian, L.; Wu, Q.; Gu, L.; Cai, S.; Wang, X.; Xiong, W.-w.; An, Z.; Huang, W. Ultralong Phosphorescence from Organic Ionic Crystals under Ambient Conditions. *Angew. Chem., Int. Ed.* **2018**, *57*, 678−682.

(8) Wu, Q.; Ma, H.; Ling, K.; Gan, N.; Cheng, Z.; Gu, L.; Cai, S.; An, Z.; Shi, H.; Huang, W. Reversible Ultralong Organic Phosphorescence for Visual and Selective Chloroform Detection. *ACS Appl. Mater. Interfaces* **2018**, *10*, 33730−33736.

(9) Wang, T.; Tang, Z.; Xu, D.; Sun, W.; Deng, Y.; Wang, Q.; Zhang, X.; Su, P.; Zhang, G. Waterborne Polyacrylates with Thermally Activated Delayed Fluorescence and Two-State Phosphorescence. *Mater. Chem. Front.* **2018**, *2*, 559−565.

(10) Yam, V. W.-W.; Au, V. K.-M.; Leung, S. Y.-L. Light-Emitting Self-Assembled Materials Based on d8 and d10 Transition Metal Complexes. *Chem. Rev.* **2015**, *115*, 7589−7728.

(11) Li, Y.; Gecevicius, M.; Qiu, J. Long Persistent Phosphors-from Fundamentals to Applications. *Chem. Soc. Rev.* **2016**, *45*, 2090−2136.

(12) Yuan, W. Z.; Shen, X. Y.; Zhao, H.; Lam, J. W. Y.; Tang, L.; Lu, P.; Wang, C.; Liu, Y.; Wang, Z.; Zheng, Q.; Sun, J. Z.; Ma, Y.; Tang, B. Z. Crystallization-Induced Phosphorescence of Pure Organic Luminogens at Room Temperature. *J. Phys. Chem. C* **2010**, *114*, 6090−6099.

(13) Bolton, O.; Lee, K.; Kim, H.-J.; Lin, K. Y.; Kim, J. Activating Efficient Phosphorescence from Purely Organic Materials by Crystal Design. *Nat. Chem.* **2011**, *3*, 205−210.

(14) Hirata, S.; Totani, K.; Zhang, J.; Yamashita, T.; Kaji, H.; Marder, S. R.; Watanabe, T.; Adachi, C. Efficient Persistent Room Temperature Phosphorescence in Organic Amorphous Materials under Ambient Conditions. *Adv. Funct. Mater.* **2013**, *23*, 3386−3397.

(15) Zhang, X.; Xie, T.; Cui, M.; Yang, L.; Sun, X.; Jiang, J.; Zhang, G. General Design Strategy for Aromatic Ketone-Based Single-Component Dual-Emissive Materials. *ACS Appl. Mater. Interfaces* **2014**, *6*, 2279−2284.

(16) An, Z.; Zheng, C.; Tao, Y.; Chen, R.; Shi, H.; Chen, T.; Wang, Z.; Li, H.; Deng, R.; Liu, X.; Huang, W. Stabilizing Triplet Excited States for Ultralong Organic Phosphorescence. *Nat. Mater.* **2015**, *14*, 685−690.

(17) Zhao, W.; He, Z.; Lam, J. W. Y.; Peng, Q.; Ma, H.; Shuai, Z.; Bai, G.; Hao, J.; Tang, B. Z. Rational Molecular Design for Achieving Persistent and Efficient Pure Organic Room-Temperature Phosphorescence. *Chem.* **2016**, *1*, 592−602.

(18) Bian, L.; Shi, H.; Wang, X.; Ling, K.; Ma, H.; Li, M.; Cheng, Z.; Ma, C.; Cai, S.; Wu, Q.; Gan, N.; Xu, X.; An, Z.; Huang, W. Simultaneously Enhancing Efficiency and Lifetime of Ultralong Organic Phosphorescence Materials by Molecular Self-Assembly. *J. Am. Chem. Soc.* **2018**, *140*, 10734−10739.

(19) Yang, J.; Zhen, X.; Wang, B.; Gao, X.; Ren, Z.; Wang, J.; Xie, Y.; Li, J.; Peng, Q.; Pu, K.; Li, Z. The Influence of the Molecular Packing on the Room Temperature Phosphorescence of Purely Organic Luminogens. *Nat. Commun.* **2018**, *9*, 840.

(20) Zhao, W.; He, Z.; Peng, Q.; Lam, J. W. Y.; Ma, H.; Qiu, Z.; Chen, Y.; Zhao, Z.; Shuai, Z.; Dong, Y.; Tang, B. Z. Highly Sensitive Switching of Solid-State Luminescence by Controlling Intersystem Crossing. *Nat. Commun.* **2018**, *9*, 3044.

(21) Huang, C.-H.; Wu, P.-J.; Chung, K.-Y.; Chen, Y.-A.; Li, E. Y.; Chou, P.-T. Room-Temperature Phosphorescence from Small Organic Systems Containing a Thiocarbonyl Moiety. *Phys. Chem. Chem. Phys.* **2017**, *19*, 8896−8901.

(22) Xu, J.; Takai, A.; Kobayashi, Y.; Takeuchi, M. Phosphorescence from a Pure Organic Fluorene Derivative in Solution at Room Temperature. *Chem. Commun.* **2013**, *49*, 8447−8449.

(23) Koch, M.; Perumal, K.; Blacque, O.; Garg, J. A.; Saiganesh, R.; Kabilan, S.; Balasubramanian, K. K.; Venkatesan, K. Metal-Free Triplet Phosphors with High Emission Efficiency and High Tunability. *Angew. Chem., Int. Ed.* **2014**, *53*, 6378−6382.

(24) Yu, Z.; Wu, Y.; Xiao, L.; Chen, J.; Liao, Q.; Yao, J.; Fu, H. Organic Phosphorescence Nanowire Lasers. *J. Am. Chem. Soc.* **2017**, *139*, 6376−6381.

(25) Kuila, S.; Rao, K. V.; Garain, S.; Samanta, P. K.; Das, S.; Pati, S. K.; Eswaramoorthy, M.; George, S. J. Aqueous Phase Phosphorescence: Ambient Triplet Harvesting of Purely Organic Phosphors via Supramolecular Scaffolding. *Angew. Chem., Int. Ed.* **2018**, *57*, 17115−17119.

(26) Goudappagouda; Manthanath, A.; Wakchaure, V. C.; Ranjeesh, K. C.; Das, T.; Vanka, K.; Nakanishi, T.; Sukumaran, S. B. Paintable Room Temperature Phosphorescent Liquid Formulations of Alkylated Bromonaphthalimide. *Angew. Chem.* **2019**, *58*, 2284−2288.

(27) Ventura, B.; Bertocco, A.; Braga, D.; Catalano, L.; d'Agostino, S.; Grepioni, F.; Taddei, P. Luminescence Properties of 1,8-Naphthalimide Derivatives in Solution, in Their Crystals, and in Co-crystals: Toward Room-Temperature Phosphorescence from Organic Materials. *J. Phys. Chem. C* **2014**, *118*, 18646−18658.

(28) Ma, H.; Shi, W.; Ren, J.; Li, W.; Peng, Q.; Shuai, Z. Electrostatic Interaction-Induced Room-Temperature Phosphorescence in Pure Organic Molecules from QM/MM Calculations. *J. Phys. Chem. Lett.* **2016**, *7*, 2893−2898.

(29) Ma, H.; Peng, Q.; An, Z.; Huang, W.; Shuai, Z. Efficient and Long-Lived Room-Temperature Organic Phosphorescence: Theoretical Descriptors for Molecular Designs. *J. Am. Chem. Soc.* **2019**, *141*, 1010−1015.

(30) Peach, M. J. G.; Williamson, M. J.; Tozer, D. J. Influence of Triplet Instabilities in TDDFT. *J. Chem. Theory Comput.* **2011**, *7*, 3578−3585.

(31) Chantzis, A.; Laurent, A. D.; Adamo, C.; Jacquemin, D. Is the Tamm-Dancoff Approximation Reliable for the Calculation of Absorption and Fluorescence Band Shapes? *J. Chem. Theory Comput.* **2013**, *9*, 4517−4525.

(32) Rangel, T.; Hamed, S. M.; Bruneval, F.; Neaton, J. B. An Assessment of Low-Lying Excitation Energies and Triplet Instabilities of Organic Molecules with an ab Initio Bethe-Salpeter Equation Approach and the Tamm-Dancoff Approximation. *J. Chem. Phys.* **2017**, *146*, 194108.

DOI: 10.1021/acs.jpclett.9b00221
J. Phys. Chem. Lett. 2019, 10, 1037−1042

(33) Adamo, C.; Jacquemin, D. The Calculations of Excited-State Properties with Time-Dependent Density Functional Theory. *Chem. Soc. Rev.* **2013**, *42*, 845−856.
(34) Laurent, A. D.; Adamo, C.; Jacquemin, D. Dye Chemistry with Time-Dependent Density Functional Theory. *Phys. Chem. Chem. Phys.* **2014**, *16*, 14334−14356.
(35) El-Sayed, M. A. Triplet State. Its Radiative and Nonradiative Properties. *Acc. Chem. Res.* **1968**, *1*, 8−16.
(36) Niu, Y.; Peng, Q.; Geng, H.; Yi, Y.; Wang, L.; Nan, G.; Wang, D.; Shuai, Z.; Li, W. MOlecular MAterials Property Prediction Package (MOMAP) 1.0: A Software Package for Predicting the Luminescent Properties and Mobility of Organic Functional Materials. *Mol. Phys.* **2018**, *116*, 1078−1090.
(37) Shuai, Z.; Peng, Q. Excited states structure and processes: Understanding Organic Light-Emitting Diodes at the Molecular Level. *Phys. Rep.* **2014**, *537*, 123−156.
(38) Shuai, Z.; Peng, Q. Organic Light-Emitting Diodes: Theoretical Understanding of Highly Efficient Materials and Development of Computational Methodology. *Natl. Sci. Rev.* **2016**, *4*, 224−239.
(39) Tomasi, J.; Mennucci, B.; Cammi, R. Quantum Mechanical Continuum Solvation Models. *Chem. Rev.* **2005**, *105*, 2999−3094.
(40) Chibani, S.; Charaf-Eddin, A.; Le Guennic, B.; Jacquemin, D. Boranil and Related NBO Dyes: Insights From Theory. *J. Chem. Theory Comput.* **2013**, *9*, 3127−3135.
(41) Frisch, M. J.; Trucks, G. W.; Schlegel, H. B.; Scuseria, G. E.; Robb, M. A.; Cheeseman, J. R.; Scalmani, G.; Barone, V.; Mennucci, B.; Petersson, G. A.; Nakatsuji, H.; Caricato, M.; Li, X.; Hratchian, H. P.; Izmaylov, A. F.; Bloino, J.; Zheng, G.; Sonnenberg, J. L.; Hada, M.; Ehara, M.; Toyota, K.; Fukuda, R.; Hasegawa, J.; Ishida, M.; Nakajima, T.; Honda, Y.; Kitao, O.; Nakai, H.; Vreven, T.; Montgomery, J. A., Jr.; Peralta, J. E.; Ogliaro, F.; Bearpark, M. J.; Heyd, J.; Brothers, E. N.; Kudin, K. N.; Staroverov, V. N.; Kobayashi, R.; Normand, J.; Raghavachari, K.; Rendell, A. P.; Burant, J. C.; Iyengar, S. S.; Tomasi, J.; Cossi, M.; Rega, N.; Millam, N. J.; Klene, M.; Knox, J. E.; Cross, J. B.; Bakken, V.; Adamo, C.; Jaramillo, J.; Gomperts, R.; Stratmann, R. E.; Yazyev, O.; Austin, A. J.; Cammi, R.; Pomelli, C.; Ochterski, J. W.; Martin, R. L.; Morokuma, K.; Zakrzewski, V. G.; Voth, G. A.; Salvador, P.; Dannenberg, J. J.; Dapprich, S.; Daniels, A. D.; Farkas; Foresman, J. B.; Ortiz, J. V.; Cioslowski, J.; Fox, D. J. *Gaussian 09* revison C.01; Gaussian, Inc.: Wallingford, CT, 2009.
(42) Gao, X.; Bai, S.; Fazzi, D.; Niehaus, T.; Barbatti, M.; Thiel, W. Evaluation of Spin-Orbit Couplings with Linear-Response Time-Dependent Density Functional Methods. *J. Chem. Theory Comput.* **2017**, *13*, 515−524.
(43) Lu, T.; Chen, F. Multiwfn: A Multifunctional Wavefunction Analyzer. *J. Comput. Chem.* **2012**, *33*, 580−592.
(44) Peng, Q.; Niu, Y.; Shi, Q.; Gao, X.; Shuai, Z. Correlation Function Formalism for Triplet Excited State Decay: Combined Spin-Orbit and Nonadiabatic Couplings. *J. Chem. Theory Comput.* **2013**, *9*, 1132−1143.

DOI: 10.1021/acs.jpclett.9b00221
J. Phys. Chem. Lett. 2019, 10, 1037−1042